43rd IEEE Conference on Decision and Control
December 14-17, 2004
Atlantis, Paradise Island, Bahamas

Electric Potential Estimation with Line-of-Sight Measurements Using Basis Function Optimization

Harish J. Palanthandalam-Madapusi, Steven Gillijns, Aaron J. Ridley,
Dennis S. Bernstein, and Bart De Moor

Abstract— **Given line-of-sight drift-velocity measurements at points on the earth, our goal is to estimate the electric potential distribution to match the drift velocity pattern. The electric potential is first expressed as a coefficient expansion of radial basis functions, and based on this expansion the expressions for the velocities are derived. A least-squares problem is then set up to minimize the error between the estimated velocity and the measurements. The coefficient vector obtained by solving the least squares problem is used to reconstruct the potential pattern. To further improve the fit, optimization of basis function parameters are also considered. Necessary gradient expressions are derived, which are then used in a quasi-Newton optimization algorithm. The new technique is demonstrated with a test problem and with real data.**

1. INTRODUCTION

The high-latitude ionospheric electric potential is a fundamental parameter that specifies the strength and pattern of magnetospheric and ionospheric convection. Variations in strong ionospheric potentials may drive large currents in power grids. Unexpected currents may disrupt consumer power by destroying transformers that were not designed to handle the externally driven currents. By predicting when these large ionospheric electric fields and strong currents may exist, power companies may take precautionary measures to reduce the power disruptions.

There are numerous methods for determining the existence of large electric fields. Since the electric field in the polar cap is tightly coupled to the Sun's atmospheric environment (or solar wind), most methodologies are based on satellite measurements approximately one hour upstream of the magnetosphere. For example, the model presented by [6] can be driven by the solar wind measurements to predict the state of the ionospheric electric field approximately one hour ahead of time.

Alternative models are based on data assimilation. There are currently two models that provide the high latitude electric field structure in real time using data assimilation, namely the SuperDARN model, and the real-time version of the assimilative mapping of ionospheric electrodynamics technique (rtAMIE). The SuperDARN model uses the empirical model described by [4] along with real time data from the suite of SuperDARN radars. Solar wind conditions are used to specify the background pattern, while the radar data are used to provide better specification. This technique is effective for determining the electric field structure because the radar measurements are assumed to be $\mathbf{V} = \mathbf{E} \times \mathbf{B}$ drifts. The configuration of the SuperDARN radars allows for the simultaneous measurement of perpendicular line of sight velocities, which can be used to fit a global electric potential pattern with few geophysical assumptions. The SuperDARN radar model can be viewed at HTTP://superdarn.jhuapl.edu/rt/map/index.html.

The assimilative mapping of ionospheric electrodynamics (AMIE) technique is one of the most important data assimilation tools in the space physics community [3, 5]. This technique uses a large (or small) number of polar data sources to produce maps of the polar electrodynamics, including the electric potential, currents, electron precipitation, and conductance. AMIE can ingest a wide variety of data including ground- and satellite-based magnetometer data, ionospheric convection data from incoherent scatter and high-frequency radars, in-situ satellites, and ionosondes, and electron particle precipitation estimates from in-situ satellites and imaging satellites. This makes AMIE one of the most versatile techniques for examining the polar electrodynamics.

One problem with both of these techniques is that they use spherical harmonics to describe the high-latitude potential patterns. This technique provides a large-scale view of the high-latitude potential and is applicable in regions where the data is spaced apart about the same distance as the resolution of the spherical harmonic functions. In locations in which the data are clustered closer than the resolution, the spherical harmonics will not be able to resolve the small spatial scales. We therefore turn to radial basis functions which can be placed at arbitrary locations, allowing a coarse or fine resolution as the data requires. Radial basis function's multi-resolution and multi-dimensional capability makes it a powerful tool for many applications [1, 2].

To test the applicability of radial basis funtion approximation, we have set up a test problem using data from the SuperDARN radar network. Each radar makes scans of the ionosphere, recieving back signals of the ionospheric velocity along the direction in which the radar is measuring. This scenario is termed line-of-sight velocity.

We represent the electric potential as a coefficient expansion of radial basis functions, and based on this expansion

This research was supported by the National Science Foundation Information Technology Research initiative, through Grant ATM-0325332 to the University of Michigan, Ann Arbor, USA

S. Gillijns and B. De Moor are with the Department of Electrical Engineering, K. U. Leuven, Belgium

A. J. Ridley is with the Space Physics Research Laboratory, University of Michigan, USA

H. J. Palanth and D. S. Bernstein are with the Department of Aerospace Engineering, University of Michigan, Ann Arbor, MI 48109-2140, USA. (734) 764-3719, (734) 763-0578 (FAX), dsbaero@umich.edu

we derive the expression for the velocity at each radar measurement point. We then set up a least-squares problem to minimize the error between the estimated velocity and the measurements. The coefficient vector obtained by solving the least squares problem is then used to reconstruct the potential pattern.

To further improve the fit, optimization of the basis function parameters is also considered. For the optimization, the gradients of the cost function with respect to the basis function parameters are derived. These gradients are then used in a standard BFGS quasi-Newton optimization algorithm.

2. Problem Formulation

We consider gaussian radial basis functions, which are of the form

$$e^{-\alpha\|x-c\|_2^2},$$

where, α determines the spread of the basis function and c determines the center of the basis function. we represent the centers of the basis functions and the points in terms of the coordinates

$$x = \begin{bmatrix} \phi\sin\theta \\ \phi\cos\theta \end{bmatrix}, \quad c = \begin{bmatrix} \phi_c\sin\theta_c \\ \phi_c\cos\theta_c \end{bmatrix},$$

where (r, ϕ, θ) for a set of spherical coordinates with the origin at the center of the earth. However, the basis functions are chosen to be functions of ϕ and θ alone, since the radius on the surface of the earth can be assumed to be constant. Choosing a set of j basis functions, we define $f \in \mathbb{R}^{1\times j}$ as

$$f \triangleq \begin{bmatrix} e^{-\alpha_1\|x-c_1\|_2^2} & e^{-\alpha_2\|x-c_2\|_2^2} & \dots & e^{-\alpha_j\|x-c_j\|_2^2} \end{bmatrix}.$$

Now, let the electric potential Φ be approximated by a basis function expansion given by

$$\Phi \approx \hat{\Phi} = fU, \tag{2.1}$$

where $U \in \mathbb{R}^{j\times 1}$ is the vector of the coefficients, $U \triangleq \begin{bmatrix} u_1 & u_2 & \cdots & u_j \end{bmatrix}^{\mathrm{T}}$. Then the electric field vector is

$$\hat{E} = -\nabla\hat{\Phi} = -\nabla f U, \tag{2.2}$$

where $\hat{E} \in \mathbb{R}^{3\times 1}$ and $\nabla f \in \mathbb{R}^{3\times j}$. Based on this electric field the drift velocity $\hat{V} \in \mathbb{R}^{3\times 1}$ can be calculated as

$$\hat{V} = \frac{\hat{E}\times B}{|B|^2}, \tag{2.3}$$

where B is the magnetic field. Now, if l is the line-of-sight vector, a least-squares problem can then be set up to minimize the error between the estimated component of the drift velocity along the line of sight of measurement $\hat{V}_l$, and the measured velocity V. Thus, the problem is to minimize the cost function

$$J(U) \triangleq (\hat{V}_l - V)^2. \tag{2.4}$$

3. Least-Squares Solution

The least-squares problem is to estimate a coefficient matrix U to minimize the cost function $J(U)$. First we derive an expression for $\hat{V}$.

The gradient ∇f in spherical coordinates is given by

$$\nabla f = \begin{bmatrix} \frac{\partial}{\partial r}f & \frac{1}{r}\frac{\partial}{\partial\phi}f & \frac{1}{r\sin\phi}\frac{\partial}{\partial\theta}f \end{bmatrix}^{\mathrm{T}}. \tag{3.1}$$

Thus, the expression for the gradient of the i^{th} radial basis function in f is

$$\nabla e^{-\alpha_i\|x-c_i\|_2^2} = \begin{bmatrix} \frac{\partial}{\partial r}e^{-\alpha_i\|x-c_i\|_2^2} \\ \frac{1}{r}\frac{\partial}{\partial\phi}e^{-\alpha_i\|x-c_i\|_2^2} \\ \frac{1}{r\sin\phi}\frac{\partial}{\partial\theta}e^{-\alpha_i\|x-c_i\|_2^2} \end{bmatrix}. \tag{3.2}$$

The components of (3.2) can be evaluated as

$$\begin{aligned} \frac{\partial}{\partial r}e^{-\alpha_i\|x-c_i\|_2^2} &= 0, \\ \frac{1}{r}\frac{\partial}{\partial\phi}e^{-\alpha_i\|x-c_i\|_2^2} &= -\frac{2\alpha_i}{r}\left[(\phi\sin\theta - \phi_{c_i}\sin\theta_{c_i})\sin\theta\right. \\ &\quad \left.+(\phi\cos\theta - \phi_{c_i}\cos\theta_{c_i})\cos\theta\right]e^{-\alpha_i\|x-c_i\|_2^2}, \\ \frac{1}{r\sin\phi}\frac{\partial}{\partial\theta}e^{-\alpha_i\|x-c_i\|_2^2} &= \frac{-2\alpha_i}{r\sin\phi}\left[(\phi\sin\theta - \phi_{c_i}\sin\theta_{c_i})\phi\cos\theta\right. \\ &\quad \left.-(\phi\cos\theta - \phi_{c_i}\cos\theta_{c_i})\phi\sin\theta\right]e^{-\alpha_i\|x-c_i\|_2^2}. \end{aligned}$$

Thus the matrix ∇f can be constructed by computing the gradient for each basis function. Once we have the gradient, the electric field vector is

$$\begin{aligned} \hat{E} &= -\nabla f U \\ &= \begin{bmatrix} 0 & \cdots \\ \frac{2\alpha_1}{r}\left[(\phi\sin\theta - \phi_{c_1}\sin\theta_{c_1})\sin\theta\right. & \cdots \\ \left.+(\phi\cos\theta - \phi_{c_1}\cos\theta_{c_1})\cos\theta\right]e^{-\alpha_1\|x-c_1\|_2^2} & \\ \frac{2\alpha_1}{r\sin\phi}\left[(\phi\sin\theta - \phi_{c_1}\sin\theta_{c_1})\phi\cos\theta\right. & \cdots \\ \left.-(\phi\cos\theta - \phi_{c_1}\cos\theta_{c_1})\phi\sin\theta\right]e^{-\alpha_1\|x-c_1\|_2^2} & \\ 0 & \\ \frac{2\alpha_j}{r}\left[(\phi\sin\theta - \phi_{c_j}\sin\theta_{c_j})\sin\theta\right. & \\ \left.+(\phi\cos\theta - \phi_{c_j}\cos\theta_{c_j})\cos\theta\right]e^{-\alpha_j\|x-c_j\|_2^2} & \\ \frac{2\alpha_j}{r\sin\phi}\left[(\phi\sin\theta - \phi_{c_j}\sin\theta_{c_j})\phi\cos\theta\right. & \\ \left.-(\phi\cos\theta - \phi_{c_j}\cos\theta_{c_j})\phi\sin\theta\right]e^{-\alpha_j\|x-c_j\|_2^2} & \end{bmatrix} U \end{aligned} \tag{3.3}$$

Now, the drift velocity is given by

$$\hat{V} = \frac{\hat{E}\times B}{|B|^2} \tag{3.4}$$

But before evaluating the cross product $E \times B$, we first convert both the quantities to cartesian coordinates. If $B = \begin{bmatrix} B_r & B_\phi & B_\theta \end{bmatrix}^{\mathrm{T}}$, then

$$B_{xyz} = \begin{bmatrix} B_r\sin\phi\cos\theta + B_\phi\cos\phi\cos\theta - B_\theta\sin\theta \\ B_r\sin\phi\sin\theta + B_\phi\cos\phi\sin\theta + B_\theta\cos\theta \\ B_r\cos\phi - B_\phi\sin\phi \end{bmatrix}$$

Writing the gradient of the basis function matrix as $\nabla f = \begin{bmatrix} \nabla f_r & \nabla f_\phi & \nabla f_\theta \end{bmatrix}^{\mathrm{T}}$, the gradient along the cartesian

directions is

$$\begin{aligned}\nabla f_{xyz} &= \begin{bmatrix} \nabla f_x \\ \nabla f_y \\ \nabla f_z \end{bmatrix} \\ &= \begin{bmatrix} \nabla f_r \sin\phi\cos\theta + \nabla f_\phi \cos\phi\cos\theta - \nabla f_\theta \sin\theta \\ \nabla f_r \sin\phi\sin\theta + \nabla f_\phi \cos\phi\sin\theta + \nabla f_\theta \cos\theta \\ \nabla f_r \cos\phi - \nabla f_\phi \sin\phi \end{bmatrix}.\end{aligned}$$

$$B_{xyz} \in \mathbb{R}^{3\times 1},\ \nabla f_{xyz} \in \mathbb{R}^{3\times j},\ \text{and}$$

$$\nabla f_x,\ \nabla f_y,\ \nabla f_z,\ \nabla f_r,\ \nabla f_\phi,\ \nabla f_\theta \in \mathbb{R}^{1\times j}$$

Therefore

$$\begin{aligned}\hat{V} &= \frac{1}{|B|^2}\begin{bmatrix} E_yB_z - B_yE_z \\ B_xE_z - E_xB_z \\ E_xB_y - B_xE_y \end{bmatrix} \\ &= \frac{1}{|B|^2}\begin{bmatrix} -B_z\nabla f_yU + B_y\nabla f_zU \\ -B_x\nabla f_zU + B_z\nabla f_xU \\ -B_y\nabla f_xU + B_x\nabla f_yU \end{bmatrix} \\ &= \frac{1}{|B|^2}\begin{bmatrix} -B_z\nabla f_y + B_y\nabla f_z \\ -B_x\nabla f_z + B_z\nabla f_x \\ -B_y\nabla f_x + B_x\nabla f_y \end{bmatrix} U \\ &= AU \end{aligned} \tag{3.5}$$

where $A \in \mathbb{R}^{3\times j}$ is

$$A \triangleq \frac{1}{|B|^2}\begin{bmatrix} -B_z\nabla f_y + B_y\nabla f_z \\ -B_x\nabla f_z + B_z\nabla f_x \\ -B_y\nabla f_x + B_x\nabla f_y \end{bmatrix}$$

Therefore the cost function $J(U)$ becomes

$$\begin{aligned}J(U) &= ((AU)_l - V)^2 \\ &= (A_lU - V)^2. \end{aligned} \tag{3.6}$$

If the line-of-sight vector makes an angle γ with the longitude at that location, then $A_l \in \mathbb{R}^{1\times j}$ can be expressed as

$$\begin{aligned}A_l &= \frac{1}{|B|^2}\left(-\cos\gamma\left[-B_x\nabla f_z + B_z\nabla f_x\right]\right. \\ &\quad \left. +\sin\gamma\left[-B_y\nabla f_x + B_x\nabla f_y\right]\right). \end{aligned} \tag{3.7}$$

The minimizing solution of (3.6) is then

$$U = (A_l^{\mathrm{T}}A_l)^{-1}A_l^{\mathrm{T}}V. \tag{3.8}$$

Further if the confidence level of each data point is known, then a weighted least squares problem can be setup with a weighting matrix W. The weighting matrix is chosen to be a diagonal matrix containing entries on the diagonal corresponding to the standard deviation of the corresponding data point. The new cost function would then be

$$J_w(U) = W^{-1}A_lU - W^{-1}V, \tag{3.9}$$

and the weighted least-squares solution is

$$U = (A_l^{\mathrm{T}}W^{-\mathrm{T}}W^{-1}A_l)^{-1}A_l^{\mathrm{T}}W^{-\mathrm{T}}W^{-1}V. \tag{3.10}$$

4. Basis-Function Optimization

In the previous section, the electric potential was calculated with a set of manually-chosen fixed basis functions. Although the least squares technique is effective, it might require a large number of basis functions for a satisfactory fit. A more efficient representation with fewer basis functions can be obtained by choosing an optimum set of basis functions. This is achieved by optimizing the basis function parameters to minimize the cost function.

To optimize the basis functions, we first derive the gradients of the cost function with respect to the basis function parameters. Then the expressions for the gradient are used in a standard BFGS quasi-Newton optimization algorithm. The steps for deriving the gradient of the cost function with respect to the parameter α_i is illustrated below, a similar procedure is followed for gradients with respect to ϕ_{c_i} and θ_{c_i}. To obtain the gradients of the cost function, we have

$$\begin{aligned}\frac{\partial}{\partial\alpha_i}J &= \frac{\partial}{\partial\alpha_i}A_lU \\ &= \frac{1}{|B|^2}\left(-\cos\gamma[-B_x\frac{\partial}{\partial\alpha_i}\nabla f_z + B_z\frac{\partial}{\partial\alpha_i}\nabla f_x]\right. \\ &\quad \left. +\sin\gamma[-B_y\frac{\partial}{\partial\alpha_i}\nabla f_x + B_x\frac{\partial}{\partial\alpha_i}\nabla f_y]\right)U \end{aligned} \tag{4.1}$$

Further,

$$\begin{aligned}\frac{\partial}{\partial\alpha_i}\nabla f_x &= \sin\phi\cos\theta\frac{\partial}{\partial\alpha_i}\nabla f_r + \cos\phi\cos\theta\frac{\partial}{\partial\alpha_i}\nabla f_\phi \\ &\quad -\sin\theta\frac{\partial}{\partial\alpha_i}\nabla f_\theta, \end{aligned} \tag{4.2}$$

$$\begin{aligned}\frac{\partial}{\partial\alpha_i}\nabla f_y &= \sin\phi\sin\theta\frac{\partial}{\partial\alpha_i}\nabla f_r + \cos\phi\sin\theta\frac{\partial}{\partial\alpha_i}\nabla f_\phi \\ &\quad +\cos\theta\frac{\partial}{\partial\alpha_i}\nabla f_\theta, \end{aligned} \tag{4.3}$$

$$\frac{\partial}{\partial\alpha_i}\nabla f_z = \cos\phi\frac{\partial}{\partial\alpha_i}\nabla f_r - \sin\phi\frac{\partial}{\partial\alpha_i}\nabla f_\phi. \tag{4.4}$$

Now,

$$\frac{\partial}{\partial\alpha_i}\nabla f_r = \begin{bmatrix} 0 & \cdots & 0 & \cdots & 0 \end{bmatrix} \tag{4.5}$$

$$\frac{\partial}{\partial\alpha_i}\nabla f_\phi = \begin{bmatrix} 0 & \cdots & \frac{\partial}{\partial\alpha_i}a & \cdots & 0 \end{bmatrix} \tag{4.6}$$

$$\frac{\partial}{\partial\alpha_i}\nabla f_\theta = \begin{bmatrix} 0 & \cdots & \frac{\partial}{\partial\alpha_i}b & \cdots & 0 \end{bmatrix}, \tag{4.7}$$

where

$$\begin{aligned}a &= \frac{-2\alpha_i}{r}\left[(\phi\sin\theta - \phi_{c_i}\sin\theta_{c_i})\sin\theta\right. \\ &\quad \left.+(\phi\cos\theta - \phi_{c_i}\cos\theta_{c_i})\cos\theta\right]e^{-\alpha_i\|x-c_i\|_2^2}, \end{aligned}$$

and

$$b = \frac{-2\alpha_i}{r\sin\phi}\left[(\phi\sin\theta - \phi_{c_i}\sin\theta_{c_i})\phi\cos\theta - (\phi\cos\theta - \phi_{c_i}\cos\theta_{c_i})\phi\sin\theta\right] e^{-\alpha_i\|x-c_i\|_2^2}.$$

We then have

$$\frac{\partial a}{\partial \alpha_i} = \frac{a}{\alpha_i}\left[1 - \alpha_i\|x-c_i\|_2^2\right],$$

$$\frac{\partial a}{\partial \phi_{c_i}} = \frac{2\alpha_i e^{-\alpha_i\|x-c_i\|_2^2}}{r}\left[\sin\theta_{c_i}\sin\theta + \cos\theta_{c_i}\cos\theta\right] + aa_c$$

$$\frac{\partial a}{\partial \theta_{c_i}} = \frac{2\alpha_i e^{-\alpha_i\|x-c_i\|_2^2}}{r}\left[\phi_{c_i}\cos\theta_{c_i}\sin\theta - \phi_{c_i}\sin\theta_{c_i}\cos\theta\right] + ab_c$$

and

$$\frac{\partial b}{\partial \alpha_i} = \frac{b}{\alpha_i}\left[1 - \alpha_i\|x-c_i\|_2^2\right],$$

$$\frac{\partial b}{\partial \phi_{c_i}} = \frac{2\alpha_i e^{-\alpha_i\|x-c_i\|_2^2}}{r\sin\phi}\left[\sin\theta_{c_i}\phi\cos\theta - \cos\theta_{c_i}\phi\sin\theta\right] + ba_c$$

$$\frac{\partial b}{\partial \theta_{c_i}} = \frac{2\alpha_i e^{-\alpha_i\|x-c_i\|_2^2}}{r\sin\phi}\left[\phi_{c_i}\cos\theta_{c_i}\phi\cos\theta + \phi_{c_i}\sin\theta_{c_i}\phi\sin\theta\right] + bb_c,$$

where

$$a_c = 2\alpha_i\left[(\phi\sin\theta - \phi_{c_i}\sin\theta_{c_i})\sin\theta_{c_i} (+\phi\cos\theta - \phi_{c_i}\cos\theta_{c_i})\cos\theta_{c_i}\right],$$

$$b_c = 2\alpha_i\left[(\phi\sin\theta - \phi_{c_i}\sin\theta_{c_i})\phi_{c_i}\cos\theta_{c_i} - (\phi\cos\theta - \phi_{c_i}\cos\theta_{c_i})\phi_{c_i}\sin\theta_{c_i}\right]$$

Thus from the above expressions, (4.5), (4.6) and (4.7) can be evaluated. Therefore the gradient of the cost function with respect to each α_i, ϕ_{c_i} and θ_{c_i} can be calculated by following the above steps.

Once the expression for the gradient is available, a standard optimization algorithm like BFGS quasi-Newton algorithm can be employed to optimize the parameters of the basis functions.

5. Test Data

In order to test the method, we developed a test problem. This test problem allows for the debugging of the code and parameter testing of the method in general. Figure 1 shows a typical ionospheric high-latitude electric potential pattern. In these figures, the center of the plot is the North magnetic pole, while the outer ring is 50° magnetic latitude. The plots are in a Sun-fixed coordinate system, such that the top of the plot is noon, while the bottom is midnight. The right side is dawn. The Earth rotates under this electric potential pattern. The two-cell pattern is due to the solar wind flowing past the Earth, dragging the Earth's magnetic field lines over the poles. The field lines return at lower latitude, resulting in a two-cell pattern where the flow is directed over the pole from the top of the plot to the bottom of the plot, then returning near the sides of the plot. The peak and valley of the potential are set to 50 kV magnitude. At each grid point, the North-South and East-West velocity components are taken. These different components can be used as line-of-sight velocities within the solver described above.

Figure 2 shows the fit of the electric potential using both components of the velocity at each grid point. This was done using 125 radial basis function specified on a uniform latitude-longitude grid. The maximum and minimum in the potential are realized to within ∼10% of the true potential. **With more basis functions, this pattern is even better specified.** Using only the North-South component of the flow (Figure 3) gives a close estimate of the electric potential pattern. Although there is some clear distortion of the potential near the magnetic pole, the size and magnitude of the potential are in very good agreement with the true potential. Using only the East-West component of the velocity vectors, (Figure 4) gives the least accurate estimate of the potential magnitude. The potential is underestimated by ∼20%. There are additional cells at lower latitude which are non-physical, although they are small in magnitude.

6. Real Data

The real ionospheric electric potential pattern is usually much more complex than the one described above, and the simplified description is correct only to zeroth order. Figure 5 shows an electric potential pattern estimated by the AMIE technique using SuperDARN line-of-sight radar data on October 1, 2002 at 00:00 UT. The pattern is mostly circular with a peak in the potential of 39 kV.

Figure 6 shows the resulting electric potential pattern from the estimation technique described above. The data points used for estimation are shown as crosses. The data is non-uniformly spaced and is concentrated in two clumps, one near noon and one near midnight. The resulting pattern is circular in shape and has approximately the same spatial size as the AMIE pattern cell.

7. Conclusions

Using line-of-sight drift-velocity measurements at points on the earth, the problem of estimating the electric potential was set up as a least-squares problem. The electric potential was assumed to be approximated by a coefficient expansion of radial basis functions, and based on this expansion, expressions for the velocity at each point were derived. These expressions were used to evaluate the least-squares solution. Further, the expressions for the gradient of the cost function with respect to the basis function parameters were also derived, which was used in an optimization code to optimize the basis function parameters. Results were demonstrated with fictitious and real data.

References

[1] J. C. Carr, W. R. Fright, and R. K. Beatson, "Surface Interpolation with Radial Basis Functions for Medical Imaging," *IEEE Transactions on Medical Imaging*, Vol. 16, No. 1, pp. 96-107, Feb-1997.

[2] J. C. Carr, R. K. Beatson, J. B. Cherrie, T. J. Mitchell, W. R. Fright, B. C. McCallum and T. R. Evans, "Reconstruction and Representation of 3D Objects with Radial Basis Functions," *Computer Graphics (SIGGRAPH 2001 proceedings)*, pp. 67-76, August 2001.

[3] A. D. Richmond, “Assimilative Mapping of Ionospheric Electrodynamics,” *Adv. Space Res.*, Vol. 12, No. 6,pp. (6)59-(6)68, 1992.
[4] J. M. Ruohoniemi and R. A. Greenwald, “Statistical Patterns of High-Lattitude Convection Obatined from Goose Bay HF Radar Observations,” *Journal of Geophysical Research*, Vol. 101, No. A10,pp. 21,743-21,763, October 1, 1996.
[5] A. D. Richmond and Y. Kamide, “Mapping Electrodynamic features of the high-latitude ionosphere from localized observations,” *J. Geophys. Res.*, Vol. 93, pp.5741, 1988.
[6] D. R. Weimer, “A flexible, IMF dependent model of high-latitude electric potential having ”space weather” applications”, *Geophys. Res. Lett.*, Vol. 23, pp.2549, 1996.

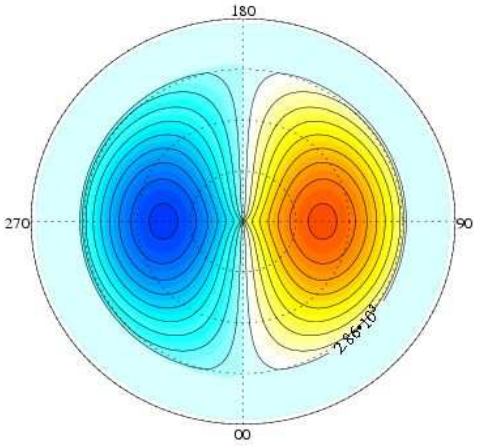

Fig. 1. Electric potential pattern for the fictitious data set.

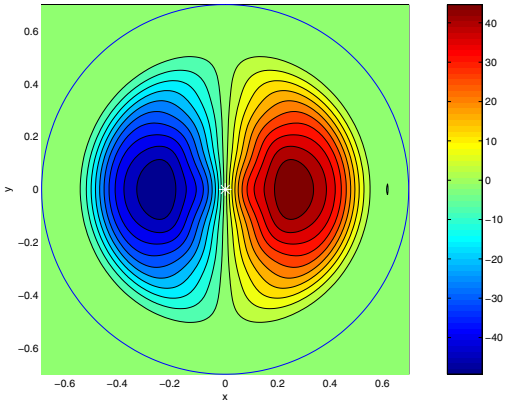

Fig. 2. Estimated electric potential pattern using both components of velocity.

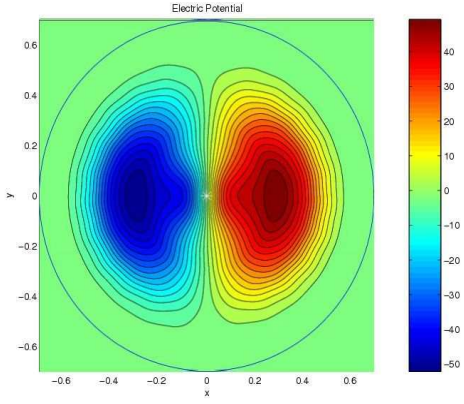

Fig. 3. Estimated electric potential pattern using only the north-south component of velocity.

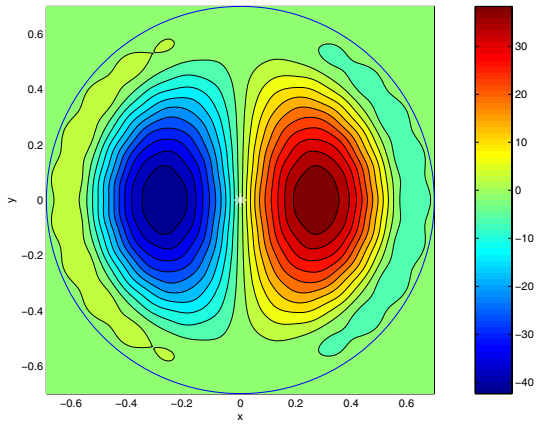

Fig. 4. Estimated electric potential pattern using only the east-west component of velocity.

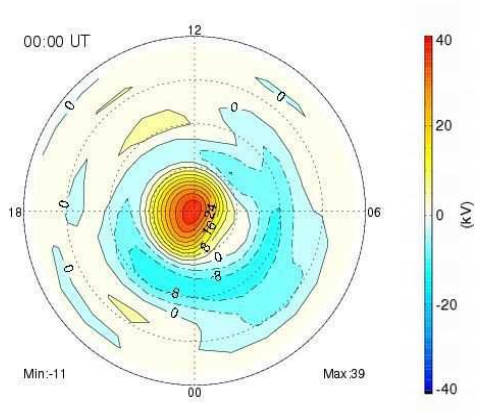

Fig. 5. Electric potential pattern for the Goose Bay data.

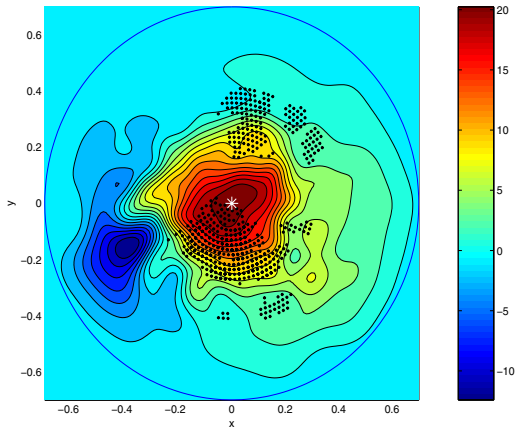

Fig. 6. Estimated electric potential pattern for the Goose Bay data.